ELSEVIER

Journal of Nuclear Materials 258–263 (1998) 1451–1457

journal of nuclear materials

Mechanical properties and microstructural characteristics of laser and electron-beam welds in V–4Cr–4Ti [1]

H.M. Chung *, J.-H. Park, R.V. Strain, K.H. Leong, D.L. Smith

Argonne National Laboratory, 9700 Cass Avenue, D-212, Argonne, IL 60439, USA

Abstract

Mechanical properties and microstructural characteristics of laser and electron-beam (EB) welds of a 500-kg heat of V–4Cr–4Ti were investigated in as-welded condition and after postwelding heat treatment (PWHT) by impact testing, microhardness measurement, optical microscopy, X-ray diffraction, and transmission electron microscopy (TEM). Ductile–brittle-transition temperatures (DBTTs) of the laser and electron-beam welds were significantly higher than that of the base metal. However, excellent impact properties could be restored in both types of welds by postwelding annealing at 1000°C for 1 h in vacuum. Analysis by TEM revealed that annealed weld zones were characterized by extensive networks of fine V(C,O,N) precipitates, which clean away O, C, and N interstitials from the grain matrices. This process is accompanied by simultaneous annealing-out of the dense dislocations present in the weld zone. This finding could be useful in identifying an optimal welding procedure by controlling and adjusting the cooling rate of the weld zone by an innovative method to maximize the precipitation of V(C,O,N).

1. Introduction

Recent research in vanadium alloys has focused on development of welding procedures and weld properties of the reference alloy V–4Cr–4Ti. A program is being conducted to develop an optimal laser welding procedure that can be applied to welding of magnetic fusion reactor structural components to be fabricated from vanadium alloy(s). Laser welds were produced on 3.8-mm-thick plates of a 500-kg heat of V–4Cr–4Ti, and mechanical properties and microstructural characteristics were investigated by several techniques in the present study. To complement the primary studies on laser welds, electron-beam (EB) welds were also investigated. In this paper, we report results of investigation of impact properties and hardening behavior of the laser and EB welds in the production-scale heat of V–4Cr–4Ti in as-welded condition and after postwelding heat-treatment (PWHT) at ≈1000°C for 1 h in high vacuum. To provide an understanding of the mechanical properties, microstructural characteristics were also investigated by X-ray diffraction, transmission electron microscopy (TEM), and chemical analysis on as-welded and postwelding-annealed specimens.

2. Experimental procedures

Compositions of the raw vanadium ingot and the V–4Cr–4Ti alloy (500-kg Heat #832665) are given in Table 1. The extruded plate was rolled and annealed several times to produce 3.8-mm-thick plates that were then annealed in the factory for ≈2 h at a nominal temperature between 1050°C and 1070°C in a diffusion-pumped vacuum furnace. The bead-on-plate laser weld was produced in air with an argon-gas purge and a 6-kW continuous CO_2 laser at a welding speed of ≈45 mm/s. Details of this procedure are reported elsewhere [1]. One-third-size Charpy impact specimens (3.3 × 3.3 × 25.4 mm, 30° notch angle, and 0.61-mm notch depth) were machined from the welded plate. The L-S orientation of the impact specimens is shown schematically in

* Corresponding author. Tel.: +1-630 252 5111; fax: +1-630 252 3604; e-mail: hee.chung@anl.gov.

[1] Work supported by the US Department of Energy, Office of Fusion Energy, under Contract W-31-109-Eng-38.

0022-3115/98/$19.00
PII: S0022-3115(98)00327-4

Table 1
Chemical composition (impurities in wppm) of industrial-scale (500-kg) heat of V–4Cr–4Ti [a] and V raw stock used to melt the ingot

Heat ID	Material	Cr	Ti	Al	Fe	Mo	Nb	Cu	Si	O	N	C	S	P	Ca	Cl	B
820630	raw V	<100	<50	100	230	410	<50	<50	800	200	62	75	10	<30	–	<2	<5
832665	alloy	3.75%	4.16%	180	180	330	<50	<50	790	280	82	64	<101	<30	<10	<2	7
		3.72%	3.79%	190	220	350	50	<50	840	360	80	80	<10	<30	<10	<2	<5
		3.83%	3.80%	105	270	260	<50	<50	720	290	93	94	<10	<30	<10	<2	<5

[a] Determined from three different positions in the 64-mm-thick and 200-mm-wide extruded bar.

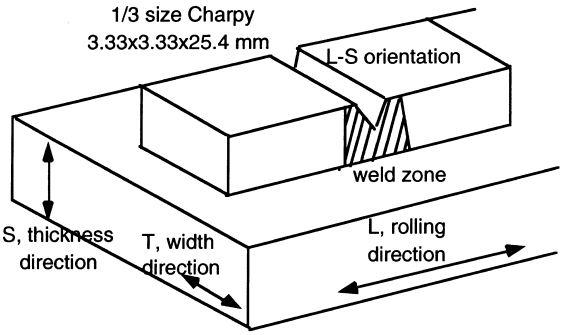

Fig. 1. Orientation of Charpy impact specimens of laser and EB welds of V–4–Cr–4Ti.

Fig. 1. Direction of crack propagation was perpendicular to the rolling direction and the flat surface of the plate. As shown, a V-notch was located in the center of the weld zone so that the crack would propagate entirely within the weld zone. The Charpy specimens machined from the weld were subjected to the customary degassing treatment at 400°C for 1 h in ion-pumped vacuum to expel hydrogen. This state of the material is referred to as the "as-welded" condition. Some of the specimens were annealed instead at 1000°C for 1 h in ion-pumped vacuum, resulting in the "postwelding heat-treated" condition. Following impact testing from −100 to 300°C, fractographic analysis and microhardness measurement were conducted on broken or bent pieces of the Charpy specimen. Vickers microhardness was measured with a 25-g load near the fracture region on one side of the Charpy specimen.

3. Impact properties and hardnening behavior

Impact properties of the laser and EB welds measured from −100 to 300°C are shown in Fig. 2; included for comparison are weld impact energies measured after degassing the machined Charpy specimens at 400°C (referred to as as-welded condition) and at 1000°C ("PWHT" condition). Impact energy of the base metal is also plotted in the figure as a function of temperature. The ductile–brittle-transition temperatures (DBTTs) of the laser and EB welds were ≈80°C and ≈30°C, respectively. These are significantly higher than the DBTTs of the base metal (≈−170°C). However, excellent impact properties with DBTTs <−80°C could be restored in both the laser and EB welds by postwelding annealing at 1000°C for 1 h. Impact energies at <−80°C could not be measured because a sufficient number of specimens were not available. True DBTTs of the postwelding-annealed laser and EB welds are probably as low as the DBTTs of the base metal.

Consistent with the effects of PWHT on impact properties, the microhardness of the laser and EB welds

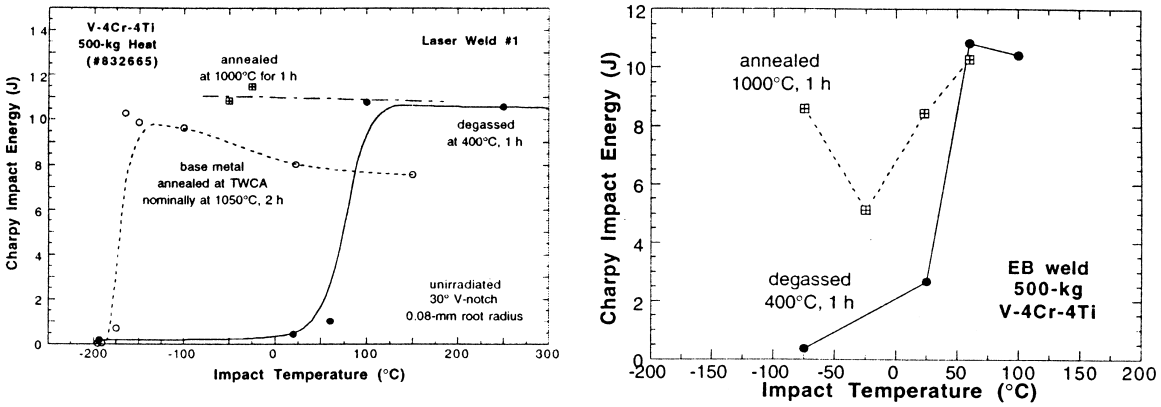

Fig. 2. Impact properties of laser (left) and EB (right) welds of V–4Cr–4Ti after annealing under various conditions.

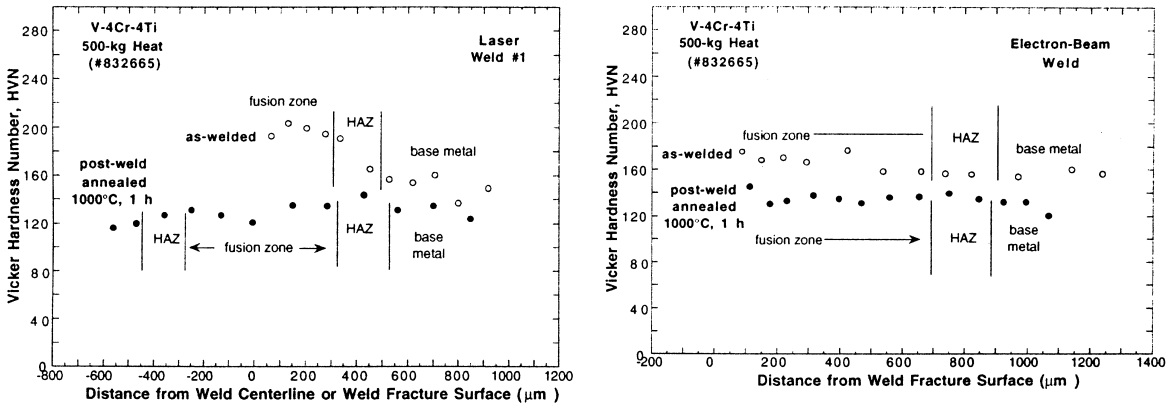

Fig. 3. Hardness profiles of laser (left) and EB (right) welds of V–4Cr–4Ti before and after annealing at 1000°C.

decreased significantly after postwelding annealing. This is shown in Fig. 3. Vickers hardnesses of the fusion and heat-affected zones (HAZ) of the laser and EB welds were ≈200 and ≈170, respectively, in as-welded condition. After the postwelding annealing, hardness decreased to ≈130. Hardness of the base metal decreased from ≈160 to ≈130 after the postwelding annealing. As expected, absorbed impact energy of the laser or EB welds seems to be more sensitive to postwelding annealing at 1000°C than hardness. To understand the PWHT behavior, microstructural characteristics were then investigated by several metallographic techniques.

4. Microstructural analyses

4.1. Optical microscopy

Optical micrographs of the as-welded and postwelding-annealed specimens of the laser weld are shown in Fig. 4. The photomicrographs were obtained from the side of the broken or bent Charpy specimens that were impact-tested after the heat treatment. In the photomicrograph of the postwelding-annealed material, a characteristic fine substructure is visible within the elongated grains of the fusion zone. This substructure is absent in the as-welded material. In EB welds, early-stage development of the similar fine substructure was observed even in as-welded material (Fig. 5). In the postwelding-annealed EB weld, the substructure appears to have developed into an advanced stage.

4.2. Chemical analysis

Concentrations of O, C, and N were analyzed in EB welds. Three specimens of base metal and three specimens of EB weld were analyzed. The concentrations were compared in Table 2 with those measured on an extruded plate (64-mm-thick) and a rolled base-metal plate (3.8-mm-thick). Compared to the composition of the rolled and annealed base-metal plate, the increase in O, N, and C in the EB welds was insignificant. There-

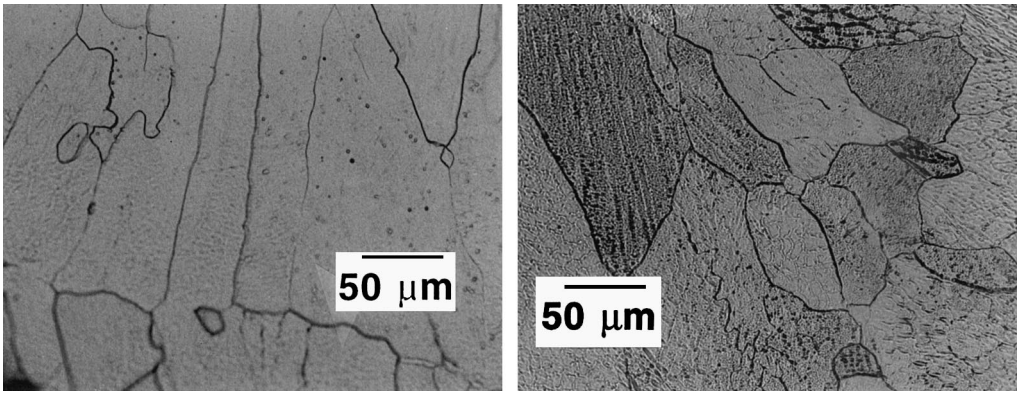

Fig. 4. Optical metallographs of laser weld of V–4Cr–4Ti in as-welded state (left) and after postwelding annealing at 1000°C for 1 h (right).

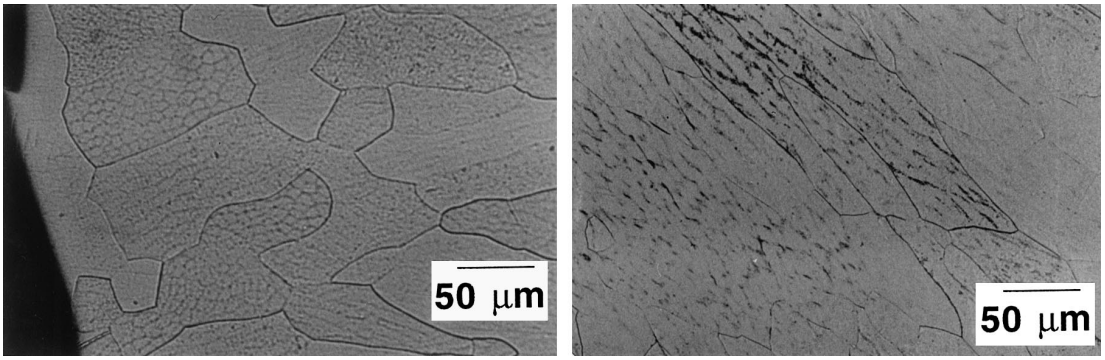

Fig. 5. Optical metallographs of EB weld of V–4Cr–4Ti in as-welded state (left) and after postwelding annealing at 1000°C for 1 h (right).

Table 2
Impurity concentration (in wppm) in 500-kg V–4Cr–4Ti Heat #832665 after extrusion, rolling and annealing, and EB welding

Fabricated material	O		N		C	
	Reading	Average	Reading	Average	Reading	Average
Extruded plate	310	310	85	85	80	80
Rolled plate	450, 480, 467	466	25, 28, 30	27	300, 230, 240	257
EB weld	510, 520, 520	517	30, 25, 29	28	240, 270, 240	250

fore, contamination by O, N, and C in the EB and laser welds appears to be at best a secondary factor in the large shifts in DBTTs before and after welding.

4.3. X-ray diffraction analysis

Tetragonal distortion was suspected initially in the crystallographic structure of the elongated grains in the fast-cooled fusion zone. However, X-ray diffraction analysis showed no evidence of tetragonal distortion; only the diffraction peaks that correspond to the bcc structure of vanadium were present, i.e., (110), (200), (211), (220), and (310). However, the lattice constant of the weld fusion zone was found to be ≈0.13% larger than that of the base metal, i.e., 0.30315 vs. 0.30275 nm, respectively. These lattice constants were then used to index the TEM diffraction patterns.

4.4. TEM analysis

As-welded microstructures of laser and EB welds were characterized by dense dislocations as shown in Fig. 6. Ti(O,N,C) precipitates normally present in extruded, rolled, and annealed plates were conspicuously

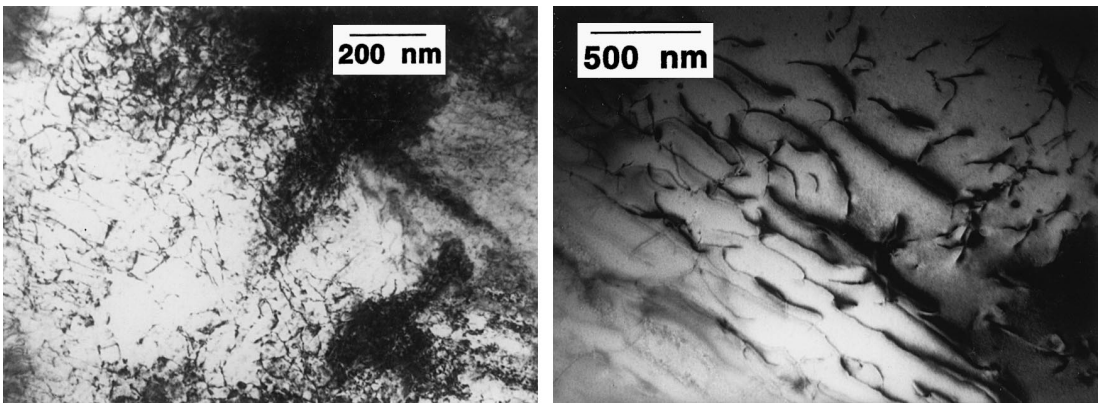

Fig. 6. TEM bright-field photomicrographs of laser (left) and EB (right) welds of V–4Cr–4Ti before postwelding annealing. Note dense dislocations and absence of Ti (O, N, C)

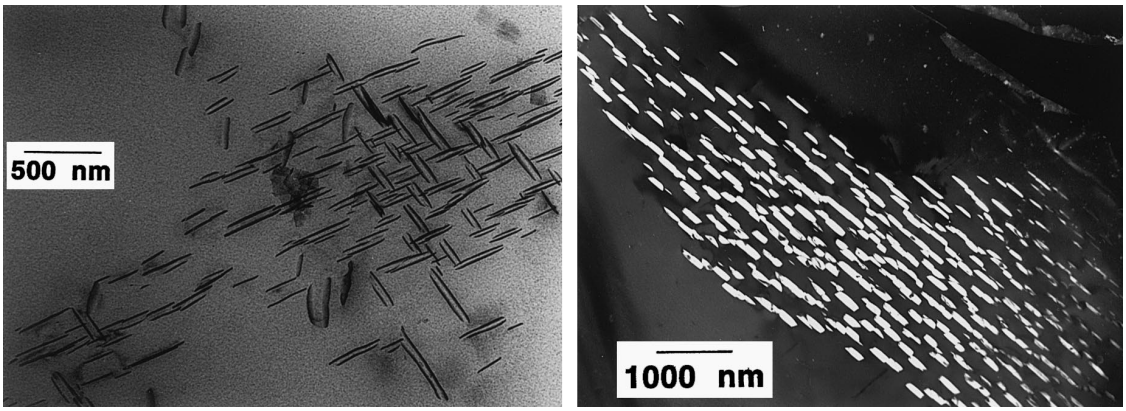

Fig. 7. Dense precipitate substructure in fusion zone of laser (left, bright-field image) and EB (right, dark-field image) welds of V–4Cr–4Ti after postwelding annealing at 1000°C for 1 h. Note absence of dislocations and Ti (O, N, C).

absent, showing that they had dissolved during welding. Reprecipitation of Ti(O,N,C) during cool-down of the weld zone was negligible. Postwelding-annealed laser and EB welds were characterized by an extensive network of precipitates that were not observed in the base metals of any vanadium alloys investigated in this program. Examples of the network precipitate structures are shown in Fig. 7 for both laser and EB welds. Individual precipitates were typically platelike in shape, 200–500 nm in diameter. The platelike morphology indicates that the precipitates are not Ti(O,N,C), which is usually spherical or ellipsoidal and 300–500 nm in diameter. The morphologies shown in Fig. 7 indicate that the precipitates in the laser and EB welds are of the same type.

To obtain a clue as to the nature of the precipitates, selected precipitates were analyzed by energy-dispersive spectroscopy (EDS). A few precipitates located at the edge of the hole of the perforated TEM foil were analyzed. The measured EDS spectrum, therefore, consisted of X-rays that originated predominantly from the precipitate, while X-rays from the alloy matrix were in minor proportion. Results of the EDS analysis of the precipitate and alloy matrix, given in Table 3, indicate that the precipitate has high concentrations of V, C, and O, and, to a lesser extent, Ti. The nitrogen signal was negligible.

However, exact compositions of C and O in this type of analysis must be considered as only qualitative, because contamination of C from the TEM vacuum chamber and hydrocarbon thinning solution is possible. Furthermore, accurate determination of C and O by EDS is complicated because the weak K lines of C and O nearly overlap the L lines of V and Ti. Therefore, exact identification of the precipitate phase must be verified by a more precise analysis through dark-field imaging and indexing selected-area diffraction patterns (SADPs). Systematic analysis of dark-field images and SADPs showed that the characteristic precipitates are V(C,O) [2], which is an fcc phase with a lattice constant of 0.419 nm. An example of the indexed diffraction patterns is shown in Fig. 8. In this pattern, one zone axis of vanadium and two zone axes of V(C,O) phase are operating. Indexed diffraction patterns obtained from the laser and EB welds showed that the precipitates formed in the two types of welds are the same V(C,O) phase. It must be emphasized that the precipitate SADPs could be indexed exactly only on the basis of the structure of V(C,O), but by no means could they be indexed on the basis of the structure of Ti(O,N,C) [3] even though the precipitates appear to contain small amount of Ti.

5. Discussion

VC (lattice constant 0.417 nm), VO (0.409 nm), and VN (0.413 nm) phases are isostructural (fcc, Na–Cl type)

Table 3
Summary of EDS analysis of composition (at.%) of characteristic precipitates in laser weld fusion zone after postwelding annealing at 1000°C for 1 h in vacuum

Material	V	Ti	Cr	C	O
Matrix	92.55	3.68	3.77	–	–
Precipitate	16.72	5.94	0.76	66.99	9.59

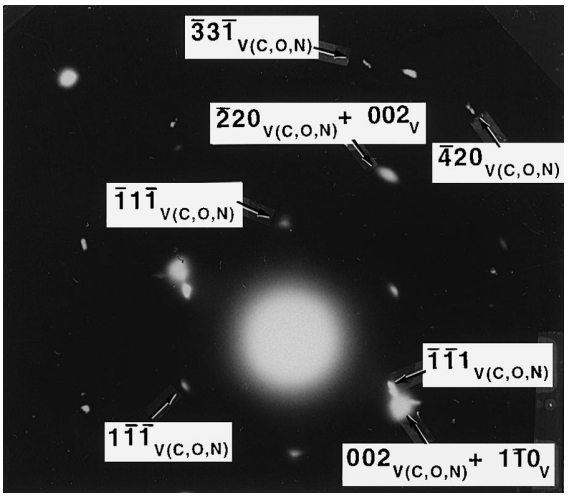

Fig. 8. Indexed selected area diffraction pattern of laser weld fusion zone of V–4Cr–4Ti postwelding-annealed at 1000°C for 1 h.

and have similar lattice constants [2] and high miscibility with one another [4]. This is similar to the characteristics of TiC, TiO, and TiN, which are also isostructural fcc with similar lattice constants and high miscibility. Therefore, as for Ti(C,O,N), the vanadium-base precipitates characteristically contained in the postwelding-annealed welds are believed to be in the chemical form of V(C,O,N), with variable proportions of C, O, and N in the precipitate. However, for the precipitate analyzed in Table 3, N content was negligible. The substructures observed in the low-magnification optical photomicrographs of Figs. 4 and 5 are indeed the same as the precipitate network shown in the high-magnification TEM photomicrographs of Fig. 7.

Vanadium-base precipitates have been observed only rarely in V–Ti or V–Cr–Ti alloys [5–7]. In the Ti-containing binary or ternary alloys of vanadium, observed precipitates are usually Ti-based phases, such as titanium oxycarbonitrides, titanium sulfides, or titanium phosphides [5]. Vanadium-base precipitates were observed only in alloys containing high levels of unusual impurities such as Cl, Ca, and Li, i.e., vanadium oxychlorides in V–5Cr–5Ti, which was melted with low-quality sponge Ti[6] and Ca-vanadate in unalloyed vanadium produced by the calcia-reduction process [6]. In an irradiated V–20Ti alloy which contained high boron, Li-vanadate was also observed [7]. As pointed out previously, from the thermodynamic standpoint, the precipitation of vanadium oxychlorides or calcium vanadates is preferred over precipitation of Ti-based precipitates in Cl- or Ca-rich alloys containing a certain level of oxygen [6].

Precipitation of V(C,O,N) seems to be preferred over precipitation of Ti(C,O,N) in a metastable structure such as the weld fusion zone. Following dissolution of Ti(O,N,C) during melting, a laser or EB weld fusion zone contains dense dislocations and higher levels of O, N, and C as interstitials in the grain matrices. It appears then that a dense dislocation structure plays an essential role in the precipitation of V(C,O,N) in the welds. The network-like distribution of clusters of the V(C,O,N) precipitates shown in Fig. 7 seems to support this premise. Under the same annealing condition at 1000°C for 1 h in high vacuum, V(C,O,N) precipitates were not observed in the factory-annealed base metal, which is relatively free of dislocations and contains the normal Ti(O,N,C) precipitates. This seems to be additional evidence that high-density dislocations play an important role in the precipitation of V(C,N,O) in the welds during postwelding annealing.

It seems evident that the drastic improvement in impact toughness is a result of the simultaneous process of profuse formation of V(C,O,N) precipitates and annealing-out of the dense dislocations that occurs in the weld zone during the postwelding annealing. The combined process seems to make grain matrices that are very low in O, C, and N and virtually free of dislocations and residual stress. Crack propagation through this type of microstructure would then be very difficult, which leads to excellent impact toughness.

The precipitation kinetics of V(C,O,N) in the metastable structure of laser welds are believed to be strongly influenced by annealing temperature. Therefore, identification of the temperature of fastest precipitation kinetics in the time-temperature-transformation (TTT) curve will be important. This temperature is probably significantly higher than 1000°C, and the kinetics at that temperature seem to be fast. This can be deduced from the observation of the early-stage development of the precipitate network in EB welds even without postwelding annealing (Fig. 5). A controlled cooling of a laser weld would then be an attractive idea to improve welding procedures and properties, in which the weld structure remains at the temperature of maximum precipitation kinetics for a reasonable period of time to allow development of networks of V(C,O,N) precipitates.

6. Conclusions

1. Hardening behavior and impact properties of laser and EB welds of V–4Cr–4Ti were investigated with and without postwelding annealing at 1000°C for 1 h in high vacuum. Ductile–brittle-transition temperatures (DBTTs) of the laser and EB welds were ≈80°C and ≈30°C, respectively, significantly higher than the DBTTs of the base metal. However, excellent impact properties could be restored in both the laser and EB welds by postwelding annealing at 1000°C for 1 h in

vacuum. Consistent with this, microhardness of the laser and EB welds decreased significantly following postwelding annealing.

2. Postwelding-annealed welds were characterized by extensive formation of networks of fine V(C,O,N) precipitates. This process occurs with simultaneous annealing-out of the dense dislocations present in the metastable fusion zone.
3. The drastic improvement in impact toughness is a result of this simultaneous process, which occurs in the fusion zone during the postwelding annealing at 1000°C for 1 h. The combined process seems to make grain matrices that are very low in O, C, and N and virtually free of dislocations and residual stress. Resistance to crack propagation through the grains of this type of microstructure is high, and as a result, excellent impact toughness is produced.
4. The precipitation kinetics of V(C,O,N) in the metastable structure of laser welds are predicted to be strongly influenced by annealing temperature, and hence by cooling history. Therefore, it seems possible to produce high-quality welds under practical conditions by controlling and adjusting the cooling rate of the weld fusion zone through some innovative method to maximize the precipitation of V(C,O,N).

Acknowledgements

The authors thank L.J. Nowicki and K. Fukumoto for extensive experimental contributions and examination of TEM specimens, respectively.

References

[1] R.V. Strain, K.H. Leong, D.L. Smith, in: Fusion Reactor Materials, Semiannual Prog. Rep. DOE/ER-0313/19, Oak Ridge National Laboratory, Oak Ridge, TN, 1995, pp. 3–4.
[2] M. Hansen, Constitution of Binary Alloys, 2nd Ed., McGraw-Hill, New York, 1958.
[3] H.M. Chung, D.L. Smith, J. Nucl. Mater. 191–194 (1992) 942.
[4] C.K. Gupta, N. Krishnamurthy, Extractive Metallurgy of Vanadium, Elsevier, Amsterdam, 1992.
[5] H.M. Chung, B.A. Loomis, D.L. Smith, in: D.S. Gelles, R.K. Nanstad, T.A. Little (Eds.), Effects of Radiation in Metals: 16th Intl. Symp., ASTM STP 1175, American Society for Testing and Materials, Philadelphia, 1993, pp. 1185–1120.
[6] H.M. Chung, J. Gazda, L.J. Nowicki, J.E. Sanecki, D.L. Smith, in: USDOE Fusion Reactor Materials Semiannual Report, DOE/ER-0313/15, 1994, pp. 207–218.
[7] H.M. Chung, B.A. Loomis, D.L. Smith, J. Nucl. Mater. 212–215 (1994) 804.